Effect of implantation of Sm^+ ions into RF sputtered ZnO thin film

Cite as: AIP Advances 9, 045210 (2019); doi: 10.1063/1.5093586
Submitted: 22 February 2019 • Accepted: 26 March 2019 •
Published Online: 10 April 2019

View Online

Export Citation

CrossMark

Francis Otieno,[1,2,3,a)] Mildred Airo,[2] Eric G. Njoroge,[4] Rudolph Erasmus,[1] Theodore Ganetsos,[5] Alexander Quandt,[1,3] Daniel Wamwangi,[1,3] and David G. Billing[1,2]

AFFILIATIONS

[1] Materials for Energy Research group, Material Physics Research Institute, School of Physics, University of the Witwatersrand, Private Bag 3, Wits, 2050 Johannesburg, South Africa
[2] School of Chemistry, University of the Witwatersrand, Private Bag 3, Wits 2050, South Africa
[3] Historical Museum of Physics and Study & Research Centre "Enrico Fermi", 00184 Roma, Italy
[4] ENGAGE, University of Pretoria, Private Bag X20, Pretoria 0028, South Africa
[5] University of West Attica, Perou Ralli & Thevon 250, Egaleo, Greece

[a)] Francis Otieno frankotienoo@gmail.com

ABSTRACT

The effects of implantation of Samarium ions (Sm^+), a rare earth ion (RE) on the properties of ZnO films grown on Si (001) substrate by RF sputtering system are presented. The structural properties of the virgin and Sm–implanted ZnO thin films were investigated by Atomic force microscopy, Rutherford backscattering spectroscopy and Raman spectroscopy. Local lattice softening caused by the incorporation of highly mismatched Sm^+ (ionic radii 0.096 nm and 0.113 nm for Sm^{3+} and Sm^{2+} respectively) into Zn antisites was detected as a red shift in E2 (high) mode likely caused by reduction in the crystallinity of the ZnO film. Photoluminescence on the pristine ZnO film showed a strong near band gap (NBE) emission and an intrinsic defect related blue, green-orange emission. The NBE is suppressed after implantation of Sm^+ while the blue, green – orange emission intensities are enhanced as a result of increased structural defects with mismatched charge states. Moreover the effect of varying the concentration of Sm^+ ions is presented and compared with predictions made from Stopping and Range of Ions in Matter (SRIM) calculation.

© 2019 Author(s). All article content, except where otherwise noted, is licensed under a Creative Commons Attribution (CC BY) license (http://creativecommons.org/licenses/by/4.0/). https://doi.org/10.1063/1.5093586

I. INTRODUCTION

Zinc oxide (ZnO) thin film has emerged as a promising candidate for transparent electronic device applications such as bottom electrode layer in solar cells, ultraviolet laser emission, photodetectors, piezoelectricity and biosensors.[1] The widespread application has been prompted by its wide direct band gap (3.3 eV), a large exciton binding energy of ~60 meV at room temperature.[2–4] These excellent properties enable its application as a light-emitter due to its efficient excitonic emission at room temperature. In addition, ZnO is also a well-known green light-emitting phosphor when excited at wavelengths below 385 nm.[5] Energy absorption occurs due to the interband transition by valence electrons to the conduction band. Recombination usually occurs close to or in the electronic defects.[6] Such defects are usually dependent on the morphology, structure, particle size, composition and crystallinity of ZnO.[7]

Doping of ZnO nanostructures with selective elements has been explored to tune its opto-electrical properties[3] through band gap engineering.[8] Among the promising materials for incorporation to the active layer in electroluminescent materials are RE ions[9] which provide intermediate emission pathways through electronic transitions to the associated energy levels. The addition of the RE can be accomplished by either ion implantation in a doping process or via physical vapor deposition technique. Hence there is need to investigate suitable doping element that enable efficient excitation of RE ions through energy transfer between the host semiconductors and the RE ions.

© Author(s) 2019

The 4f levels of triply charged rare-earth ions have a wide range of applications such as lasers, phosphors and luminophors.[10] The use of electron impact to excite ions when incorporated into a semiconducting matrix has attracted much interest because of these numerous applications owing to the stability of the semiconducting oxides. However, the doping has had its own share of challenges such as low saturated concentration of RE ions in ZnO lattice due to the large differences in ionic size and mismatch in the charge state and the inappropriate energy level position of RE ion relative to the valence band and conduction band of ZnO host.[11]

There is still need to evaluate the composition, structure and optical properties of ZnO thin films after RE addition. Additionally the choice of the RE atom and its crystalline environment in these doped metal oxides must satisfy the optimum requirements for the diverse photonic applications.

II. EXPERIMENTAL PROCEDURE

A. Growth of ZnO thin film

ZnO disk (99.99% purity) targets of diameter 76 mm and thickness 6 mm sourced from Semiconductor Wafer, Inc. (SWI) were used for thin film deposition in RF magnetron sputtering system. The Si wafer (001) substrates were also purchased from Semiconductor Wafer, Inc. (SWI). The RF system vacuum chamber was evacuated using a rotary roughing pump to a base pressure of 2×10^{-2} mbar before a further pumping using turbo-molecular pump to 1.8×10^{-5} mbar. The plasma generation chamber was surrounded by an electromagnet. Magnetron sputtering was carried out in an argon gas atmosphere supplied into the chamber through a constant precision leak valve at a flow rate of 13.0 sccm. Herein, we report the structural and optical behavior of Sm-doped ZnO thin films before and after implantation of Sm^+ ions at different dose rates using a Varian 200-20A2F ion implanter located at iThemba LABS (Gauteng) operated at energy of 80 keV.

B. Sm ion implantation

The Sm^+ ions were produced from a cut piece of a Sm_2O_3 sputter target (99.99% purity, sourced from SWI) and extracted as incident ions for implantation into pristine ZnO thin film through charge to mass ratio using a Varian 200-20A2F ion implanter located at iThemba LABS (Gauteng), Johannesburg at room temperature at high vacuum. SRIM programme was first used before ion implantation to project the composition and distribution profiles of the Sm^+ in ZnO matrix.

C. Thin film characterization

The film morphologies and structural analyses were characterized using Veeco Di-3100 atomic force microscopy (AFM) in tapping mode. Optical reflectance to attain thickness, and refractive index were analyzed using FR-Basic-VIS/NIR fitted with FR-Monitor software for fittings.

Rutherford backscattering spectrometry (RBS) measurements were performed to determine the thickness and distribution profiles of Sm^+ ions in the ZnO matrix at room temperature using $4He^+$ particles of energy 1.6 MeV at a backscattering angle of 165° (IBM geometry). The beam current was kept between 10 and 15 nA during measurements. The Raman bands and the structural order of all the films were examined using a Horiba LabRAM HR Raman spectrometer equipped with an Ar ion laser (514.5 nm) and a laser power of <1 mW at the sample. Photoluminescence measurements were carried out using a Horiba LabRAM HR spectrometer with a 150 lines/mm grating and an excitation wavelength of 244 nm from a frequency doubled Lexel argon ion laser.

III. RESULTS AND DISCUSSION

A. Stopping and range of ions in matter (SRIM) calculation

SRIM is based on a Monte Carlo simulation method, namely the binary collision approximation with a random selection of the impact parameter of the next colliding ion. SRIM is capable of producing quick calculations that produce tables of stopping powers, range and straggling distributions for any ion at any energy (in the range 10 eV–2 GeV) and in any elemental target.[12]

SRIM calculates the backscattered and sputtered particle distribution functions resulting from positive atomic- ion bombardment of any amorphous surface. When an ion bombard a solids with energetic particles, the target material's surfaces is eroded. This erosion rate quantified as the sputtering yield, defined as the average number of atoms leaving the surface of a solid per incident particle. It has been shown that the penetration depth can be expressed in terms of the parameters characterizing the target material and the incoming ion energy described by equation 1:

$$a(\epsilon) = \frac{1-m}{2m}\gamma^{m-1}\frac{\epsilon^{2m}}{nC_m} \quad (1)$$

where n is the target atom density, γ is a constant of the order of unity, C_m is a constant dependent on the parameters of the

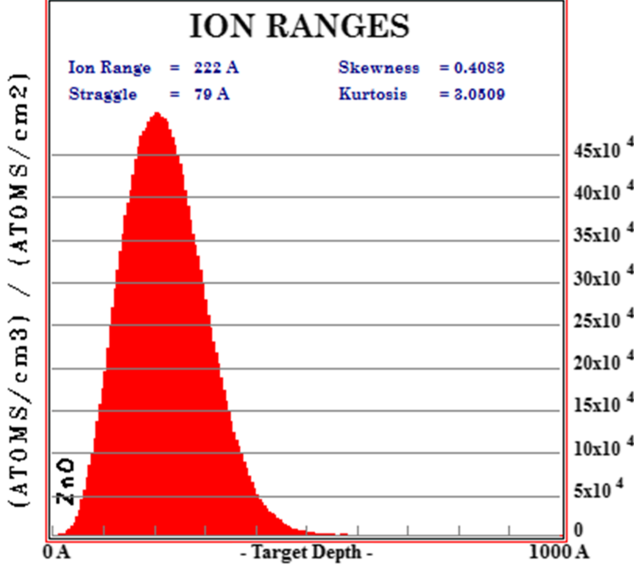

FIG. 1. SRIM profile illustrating the estimated ion distribution with penetration depth.

© Author(s) 2019

TABLE I. SRIM simulated Sm^+ concentration using varied fluence doses.

Fluence (ions/cm^2)	Mean depth (nm)	Max. concentration %	Average concentration %
2×10^{15}	20.01	1.22	0.77
4×10^{15}	20.01	2.45	1.55
6×10^{15}	20.01	3.67	2.33
8×10^{15}	20.01	4.90	3.11
1×10^{16}	20.01	6.12	3.89

inter-atomic interaction potential and m=m (ϵ) is a factor, which varies slowly from m = 1, at high energies, to m = 0, at very low energies.[13] In this project SRIM was used to estimate the ion distribution of RE (Sm^+ ions) implanted at various fluences. The substrate used in the simulation was silicon wafer of thickness ~2000 nm and the results is shown in Figure 1. The Sm profile determined by SRIM simulation shows a defined peak at approximately 20 nm and a maximum Sm ion concentration of 1.22% and 6.12% at a fluence of 2×10^{15} and 1×10^{16} ions/cm^2 respectively as shown in Table I.

The concentration of the Sm ions is seen steadily increasing with fluence as similar to RBS experimental results reported in Figure 5.

B. Morphology studies using atomic force microscopy

Figure 2 shows the surface topography of ZnO layer before and after Sm^+ implantation characterized by the Veeco Di3100 AFM in tapping mode.

From Table II, the roughness, rms of the ZnO film surface was 5.29 nm with an average grain size of 22.4 nm. Upon ion implantation of Sm^+ at a fluence of 2×10^{15} ions/cm^2, the rms increases to 17.5 nm with an average grain size of 61.1 nm. The increase in the surface roughness is attributed to the competition between ad atom diffusion and energy dissipation on the film. As the implanted dose of Sm^+ increases the surface roughness increases steadily as a result of formation of microvoid structures.[14]

During the early stages of ion implantation process, the rms roughness increases from 5.29 nm for the virgin sample to 33.3 nm after implanting with a fluence of 8×10^{15}. However, at a fluence of 10×10^{15} the roughness decreases to about 26.2 nm. During low fluences, the coarsening of nano dots makes the surface to become rougher whereas when the fragmentation and inverse-coarsening of the nanoparticles occurs at 10×10^{15}, a slight smoothening in the surface is observed.[15] According to Paramanik, Dipak, et al., smoothening of surface beyond certain fluence may be associated with amorphization of the surface. At high fluences, there is an increase in the density of electronic excitations hence the covalent bonds in the lattice weaken or get broken leading to relaxation causing the surface morphization[16,17] or reduced strain in the film.[18] It is also worth noting that the grains sizes appear larger than average particle size estimated using Debye-Sherrer relation on XRD Bragg reflexes which gave a particle size of 22.4 nm for the virgin ZnO and 61.1 nm for the ZnO implanted with Sm^+ at a fluence of 2×10^{15} ions/cm^2. As the fluence increased there is coarsening and the particles appear larger as can be seen from the increasing grain height. At a fluence of 10×10^{15} ions/cm^2 there is a decrease in grain height suggesting that the inverse ripening may be happening as a result of the fragmentation of particles.[15]

The film thickness was estimated to be about 154.8 nm using FR-Basic-VIS/NIR fitted with FR-Monitor software for fittings and did not show any reasonable change with increased fluence dose.

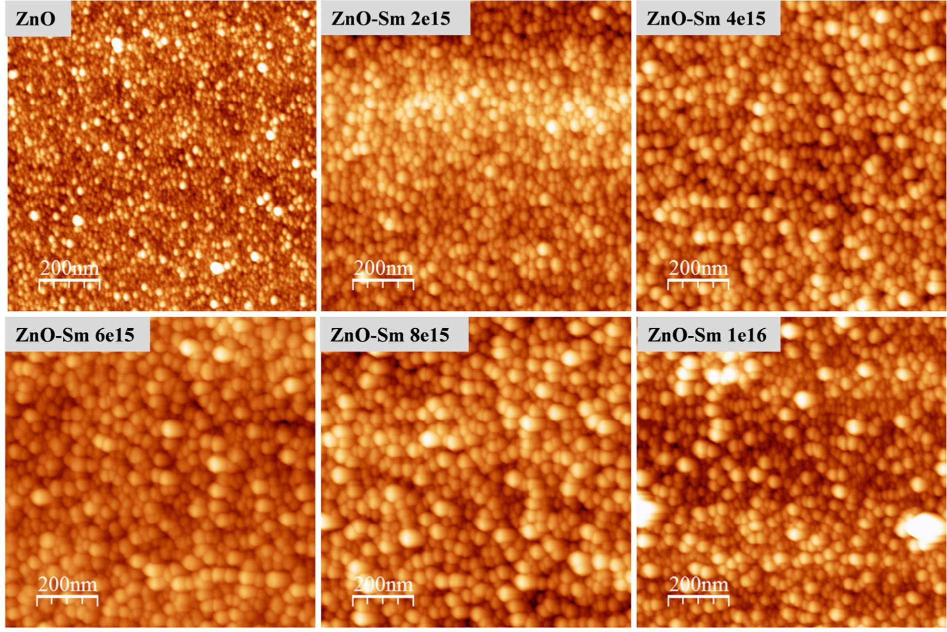

FIG. 2. Tapping mode AFM images of ZnO and ZnO:Sm thin films.

© Author(s) 2019

TABLE II. Statistical AFM analysis of the film.

Samarium fluence (ions/cm^2)	R_a (nm)	R_{rms} (nm)	Skewness (R_{sk})	Grain height (nm)
0	3.92	5.29	1.454	22.4
2×10^{15}	13.9	17.5	0.253	61.1
4×10^{15}	20.7	25.8	0.308	70.9
6×10^{15}	21.9	27.8	0.463	84.5
8×10^{15}	26.7	33.3	0.304	87.0
10×10^{15}	20.8	26.2	0.752	62.7

The elemental compositions of the films were first determined using Energy-dispersive X-ray spectroscopy measurements. The EDS (not shown here) showed that ZnO films had no impurity while the presence of Sm^+ upon implantation was only marked as RE, hence unable to differentiate RE ions with close energies that caused overlap. We therefore studied the films using Rutherford Backscattering Spectroscopy measurements as discussed in section III D.

C. VIS/NIR measurements

Figure 3 shows visible/near infrared spectroscopy of ZnO thin implanted with Sm^+ ions at a fluence of 2×10^{15} ions/cm^2 as well the refractive index measurements at a wavelength range of 450-900 nm.

Figure 3 shows reflectance curves for the ZnO thin film implanted with Sm^+ ions, where the film due to interference phenomena between the wave fronts generated at the two interfaces (air and substrate) describes the sinusoidal nature of the curves' reflectance vs. wavelength of light. ZnO thin film showed interference fringe pattern in transmission spectrum. From the spectrum, the film shows a smooth reflecting surface without much scattering loss at the surface. The thickness simulated using FR-monitor was found to be 154.8 nm which is in complete agreement with the value derived from RBS simulation and did not change by reasonable margin upon variation of the fluence dose during ion implantation. The refractive index value is seen to decrease with the increasing of the wavelength.

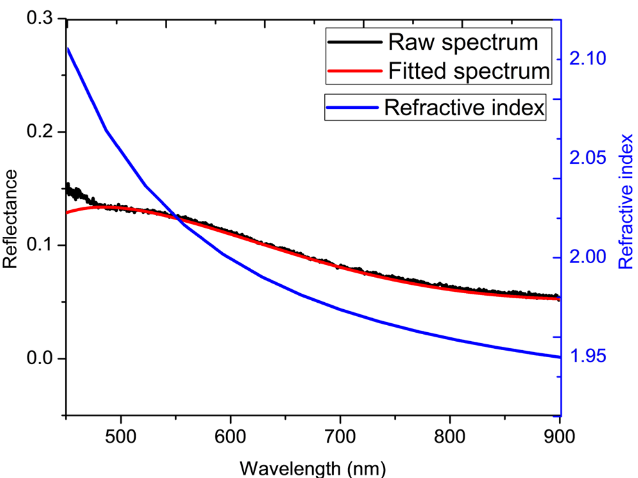

FIG. 3. Reflectance (both raw and fitted spectrum) and refractive index variation with wavelength range of 450-900 nm.

D. Rutherford backscattering spectroscopy measurements

A RBS spectrum of virgin ZnO and Sm - doped ZnO thin film at a fluence of 2×10^{15} ions/cm^2 on Si substrate is shown in Figure 4. Each experimental spectrum could well be reproduced together with a computer simulation using the XRump code. The structure in the Si spectrum around channel 180, 260, 410 and 480 are attributed to the non-Rutherford scattering cross-section from O, Si, Zn and Sm respectively and the surface energy positions in channels of the elements have been shown using arrows.

The simulated spectra yield an average thickness of the films 154 ± 2 nm in agreement with the thickness measurement by the FR-Basic-VIS/NIR fitted with FR-Monitor software for fittings.

The presence of Sm^+ in the films is quite evidenced and the global atomic concentrations of the different species contained in the film can be deduced. From the XRump simulation for Sm doped ZnO shown in Figure 4, stoichiometry of the matrix of 49.3, 48.3 and 2.37% for Zn, O and Sm, respectively was derived.

The simulated spectrum shown in Figure 4 for the minimum fluence of 2×10^{15} ions/cm^2 implantation was generated by assuming a three layer structure with the Sm^+ concentration in the layers progressively decreasing; viz. layer I with width 11 nm, layer II width 19 nm and layer III with width 124. The atomic surfaces were determined to be in channels: Zn = 401, Sm = 461, Si = 287, O = 180. The measured depth profiles slightly differ from those simulated by SRIM for the due to the fact that the SRIM code does not take

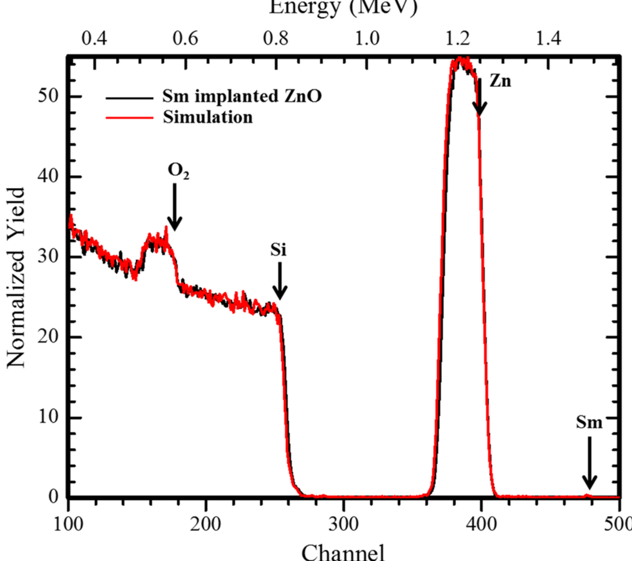

FIG. 4. RBS spectrum of an 154 nm Sm^+ implanted ZnO layer at a flunce of 2×10^{15} ions/cm^2 on 2000 nm thick Si showing experimental data and computer simulation using XRump code.

© Author(s) 2019

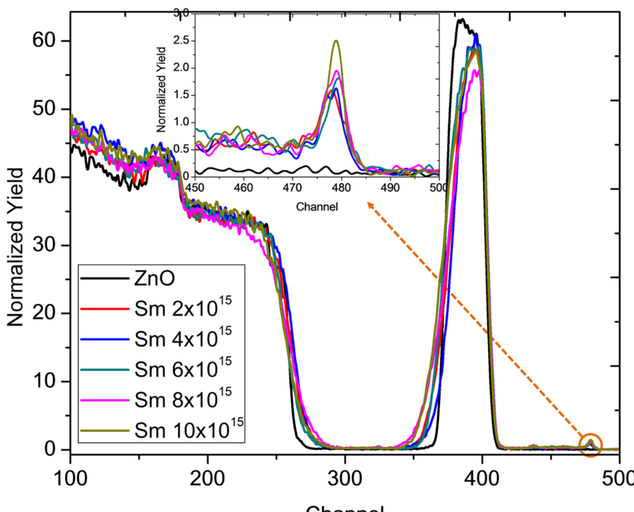

FIG. 5. RBS spectra of Sm implanted ZnO layer at different fluences at energy of 80 keV. Inset is a zoom plot of channel range 450-500.

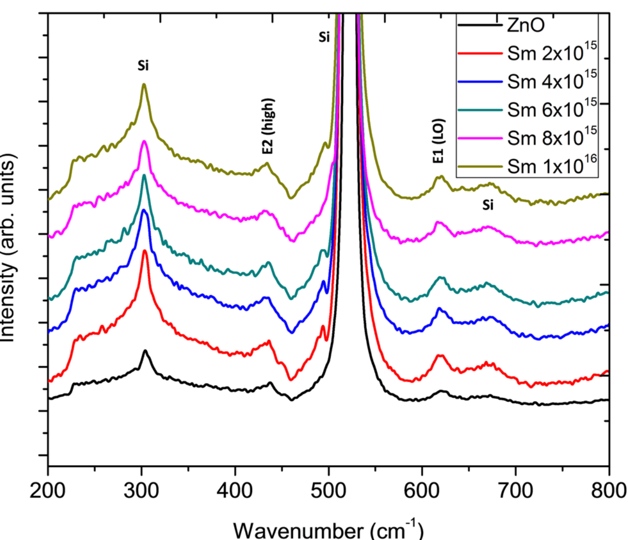

FIG. 6. Raman spectra of virgin RF sputtered ZnO films grown on Si (001) and after ion implantation with Sm^+ at different fluences.

into account progressive structural and compositional changes in the ZnO matrix caused by ion irradiation.

Figure 5 shows RBS spectrum (raw data) of the virgin and Sm-implanted ZnO films on Si substrate with the constituent atoms at different energy channels to confirm the composition depth profile and thickness of the deposited films.

From Figure 5 the Sm^+ profile was found to be almost Gaussian in shape with a maximum depth around 20 nm. This is in agreement with the projected range calculated for 80 keV Sm^+ in ZnO using the SRIM simulation – a Monte Carlo simulation based on the binary collision approximation. The normalized yield is observed to gradually increase for all fluence, an indication that the implanted Sm^+ ions were quite below saturation point. The pronounced increase of the scattering ions yield (RBS yield) around 461 channel compared with that in the virgin sample maybe an indication that implantation-induced damaging of the ZnO crystal lattice suppressing the channelling effect causing an increase of the RBS yield within the modified ZnO layer.

E. Raman spectroscopy

Figure 6 shows the Raman spectra for virgin and Sm^+ implanted ZnO thin films. ZnO crystallizes in the wurtzite structure, which belongs to the space group $C_{6V}{}^4$. According to group theory prediction its phonon modes belong to the $2E_2$, $2E_1$, $2A_1$ and $2B_1$ symmetries. The two B_1 symmetry modes are not Raman active.[19]

The room temperature Raman spectra of ZnO and Sm-doped ZnO thin films at a wavenumber of 200 to 800 cm^{-1} are shown in Figure 6. The A1 and E1 modes are polar phonons which split into transverse optical (TO) and longitudinal optical (LO) phonons. The nonpolar E_2 modes have two frequencies, namely, E_2 (low) and E_2 (high) which corresponds to the Zn and O sublattice vibrations, respectively.[20,21] In our case since the measurement was carried out between 200 to 800 cm^{-1} only the E_2 (high) was observed for both undoped ZnO (at 435.3 cm^{-1}) and Sm- doped ZnO at (431.3 cm^{-1}) using a fluence of 2×10^{15} cm^2. This E_2 (high) mode is known to be sensitive to the stress within ZnO nanostructures.[22] This peak also appears broader (FWHM value is 14.2 $cm^{-1}$for illustration) upon implantation with Sm^+ ions compared to FWHM value of 13.4 cm^{-1} for the undoped ZnO. The frequency red shift may be attributed to the local lattice softening caused by the incorporation of highly mismatched (charge state imbalance and mass) Sm^+ into Zn antisites. Softening of the lattice is caused by the large sized Sm^+ ion sitting in a strongly electronegative environment as a result of the negatively charged surrounding oxygen ions.[23,24] Since SmZn has four nearest oxygen atoms neighbors, the mode softening for the E2 (high) mode is most likely.

The intensity of the E2 (high) mode denotes the crystallization of ZnO crystal structure,[25] hence Sm-doped ZnO thin films is obviously having lower intensity compared to that of ZnO, revealing the restrained degree of crystallization along the c-axis. The possible emergence of the fiber texture along the (103) reflex in the implanted films could also lead to the suppression in the intensity of the Raman mode. The band at 580 cm^{-1} is usually defect related and is assigned to E1(LO) mode and its presence in both films indicates the presence of oxygen vacancies or oxygen interstitials.[26]

F. Photoluminescence studies

The photoluminescence properties of the ZnO and Sm-doped ZnO films are examined using room temperature photoluminescence (PL) spectroscopy fitted with an excitation source at 224 nm. Figure 7 shows explicitly distinct emissions UV emission (378.8 nm for virgin ZnO thin films and 379.7 nm for Sm - doped ZnO using fluence of 2×10^{15} cm^2) resulting from the free excitons recombination through an exciton-exciton collision process corresponding to the near-band edge (NBE) exciton emission of the wide band gap ZnO.[27,28] The red-shift in the NBE emission upon implanting Sm^+

© Author(s) 2019

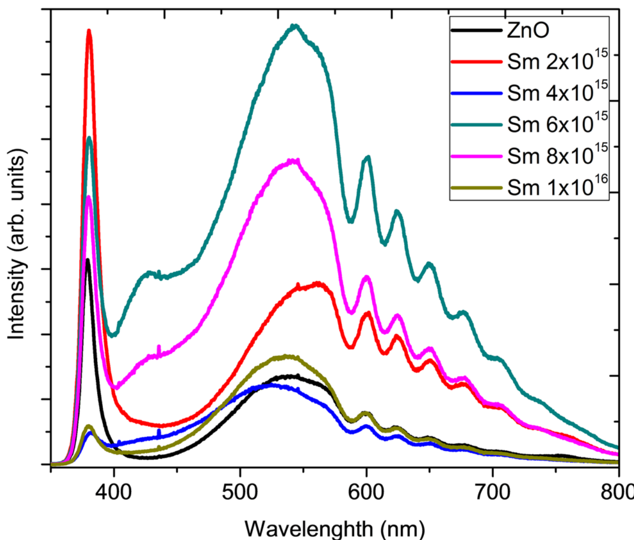

FIG. 7. Room temperature PL spectra of the ZnO and Sm^+-doped ZnO thin films both of average thickness of 154 nm.

into ZnO could possibly indicate the narrowing of the band gap due to increased dopant states near the bottom of the conduction band[14] or the prevalence of vibronic states that act as exciton recombination pathways.

The broad green emission band range in the vicinity of 560 nm is associated with the various deep-level defects, such as zinc interstitial (Zn_i), oxygen interstitial (O_i), zinc vacancy (V_{Zn}), oxygen vacancy (V_O), or single-ionized oxygen vacancies in ZnO.[29] In addition there are yellow-orange emission bands induced from the recombination of a photogenerated hole with an electron that belongs to a singly ionized defect, such as oxygen vacancy or oxygen interstitial. Upon doping with Sm^+, the possible substitution of Zn^{2+} site with low concentration Sm^+ may enhance lattice distortion to compensate for the charge imbalance and increase in the amounts of defects such as oxygen vacancies and oxygen interstitials leading to enhancement of the intensity of green, yellow and orange emission. These increased defects however led to the suppressing of the excitonic emission resulting in decrease of the NBE edge emission intensity as the fluence increased beyond 4×10^{15} cm^2.

Previous studies have been reported on PL properties of Sm^+ in ZnO polycrystalline pellets and microstructure.[11,30,31] They reported that Sm^+ photoluminescence were only observed under the direct excitation or an impact excitation by hot electrons but no energy transfer from ZnO to Sm^+ ions. However, according to Tsuji, Takahiro, *et al*[9] Sm PL properties may depend on extrinsic effects since the ZnO:Sm polycrystalline samples contain several grain boundaries and defects which usually act as non-radiative centers. In our study we noted an additional shoulder at 427 nm which could be attributed to $^4G_{5/2}$–^6F_J (J = 11/2, 9/2, 7/2, 5/2) transition of Sm^+ ions as well as a mere defects formation during ion implantation hence need for further investigation using time-resolved photoluminescence spectroscopy.

IV. CONCLUSION

The effects of implantation of Samarium ions (Sm^+) on the properties of ZnO films grown on Si (001) substrate by RF sputtering system are presented. The films showed uniformly distributed homogeneous grains, an indication of the high packing density of the films. Atomic force microscope (AFM) and the Photoluminescence (PL) were employed to analyze the influence of the Sm^+ ions implantation into the ZnO matrix. The structural properties of undoped and Sm- doped ZnO thin films were investigated by Atomic force microscopy, Scanning Electron microscopy and Raman scattering studies. Local lattice softening caused by the incorporation of highly mismatched Sm^+ into Zn antisites was detected as a red shift in E2 (high) mode and reduction in the crystallinity of the ZnO film. Photoluminescence on the pristine ZnO film has shown a strong NBE emission and an intrinsic defect related blue, green-orange emission. The NBE is suppressed after implantation of Sm^+ while the blue, green – orange emission intensities are enhanced as a result of increased structural defects with mismatched charge states. The fluence was varied and the experimental data trend was in agreement with the projected range calculated for 80 keV Sm^+ in ZnO using the SRIM simulation although the percentage composition values differ.

ACKNOWLEDGMENTS

The authors would like to thank the University of the Witwatersrand, Material Physics Research Institute, School of Physics; the XRD and MMU facilities at Wits, NRF and Material Energy Research Group (MERG) for funding. Special thanks to GCRF-START: Synchrotron Techniques for African Research and Technology for postdoctoral funding and Erasmus+ office for support to carry out optical measurements at the University of West Attica, Athens – Greece.

REFERENCES

[1] P. Velusamy, R. R. Babu, and K. Aparna, "Effect of Sm doping on the physical properties of ZnO thin films deposited by spray pyrolysis technique," AIP Conference Proceedings 080085 (2017).

[2] D. Alsebaie, W. Shirbeeny, A. Alshahrie, and M. S. Abdel-Wahab, "Ellipsometric study of optical properties of Sm-doped ZnO thin films Co-deposited by RF-magnetron sputtering," Optik-International Journal for Light and Electron Optics **148**, 172–180 (2017).

[3] W. E. Mahmoud, A. Al-Ghamdi, S. Al-Heniti, and S. Al-Ameer, "The influence of temperature on the structure of Cd-doped ZnO nanopowders," Journal of Alloys and Compounds **491**, 742–746 (2010).

[4] W. E. Mahmoud and A. Al-Ghamdi, "The influence of Cd (ZnO) on the structure, optical and thermal stabilities of polyvinyl chloride nanocomposites," Polymer Composites **32**, 1143–1147 (2011).

[5] S. Lima, F. Sigoli, M. Jafelicci, Jr., and M. R. Davolos, "Luminescent properties and lattice defects correlation on zinc oxide," International Journal of Inorganic Materials **3**, 749–754 (2001).

[6] G. Blasse and B. Grabmaier, "A general introduction to luminescent materials," in *Luminescent materials*, Springer pp. 1–9 (1994).

[7] F. A. Sigoli, C. de Oliveira Paiva-Santos, M. Jafelicci, and M. R. Davolos, "Study of crystallite size and strain as a function of morphological evolution in zinc oxide powder obtained from hydroxycarbonate precursor," Powder Diffraction **16**, 153–159 (2001).

[8] H. He, J. Fei, and J. Lu, "Sm-doping effect on optical and electrical properties of ZnO films," Journal of Nanostructure in Chemistry **5**, 169–175 (2015).

© Author(s) 2019

[9]T. Tsuji, Y. Terai, M. hakim bin Kamarudin, M. Kawabata, and Y. Fujiwara, "Photoluminescence properties of Sm-doped ZnO grown by sputtering-assisted metalorganic chemical vapor deposition," Journal of Non-Crystalline Solids **358**, 2443–2445 (2012).

[10]D. Kouyate, J.-C. Ronfard-Haret, and J. Kossanyi, "Electroluminescence of Sm^{3+} ions in semiconducting polycrystalline zinc oxide," Journal of Materials Chemistry **2**, 727–732 (1992).

[11]X. Zeng, J. Yuan, and L. Zhang, "Synthesis and photoluminescent properties of rare Earth doped ZnO hierarchical microspheres," The Journal of Physical Chemistry C **112**, 3503–3508 (2008).

[12]S. Martinie, T. Saad-Saoud, S. Moindjie, D. Munteanu, and J.-L. Autran, "Behavioral modeling of SRIM tables for numerical simulation," Nuclear Instruments and Methods in Physics Research Section B: Beam Interactions with Materials and Atoms **322**, 2–6 (2014).

[13]A. Yen, W.-k. Chu, S. Tavares, J. Arruda-Neto, M. Goncßalves, V. Likhachev, J. Mesa, E. de Oliveira, S. de Pina, and O. Rodriguez, "Subject index of volumes 211–220," Nuclear Instruments and Methods in Physics Research B **219**, 92–121 (2004).

[14]S. Eshghi, M. H. Zadeh, M. Yari, and E. Jafari-Khamse, "The effect of nitrogen ion implantation on the corrosion resistance and microstructure of tantalum-coated stainless steel," The European Physical Journal Plus **129**, 117 (2014).

[15]D. Paramanik, S. Majumder, S. Sahoo, and S. Varma, "Nano pattern formation and surface modifications by ion irradiation," Defence Science Journal **59**, 413 (2009).

[16]C. A. Volkert, "Stress and plastic flow in silicon during amorphization by ion bombardment," Journal of Applied Physics **70**, 3521–3527 (1991).

[17]P. Srivastava, V. Ganesan, and O. Sinha, "Evidence of plastic flow and recrystallization phenomena in swift (~100 MeV) Si^{7+} ion irradiated silicon," Nuclear Instruments and Methods in Physics Research Section B: Beam Interactions with Materials and Atoms **222**, 491–496 (2004).

[18]S. Dey, C. Roy, A. Pradhan, and S. Varma, "Raman scattering characterization of Si (100) implanted with mega-electron-volt Sb," Journal of Applied Physics **87**, 1110–1117 (2000).

[19]R. Al Asmar, J. Atanas, M. Ajaka, Y. Zaatar, G. Ferblantier, J. Sauvajol, J. Jabbour, S. Juillaget, and A. Foucaran, "Characterization and Raman investigations on high-quality ZnO thin films fabricated by reactive electron beam evaporation technique," Journal of Crystal Growth **279**, 394–402 (2005).

[20]J. Calleja and M. Cardona, "Resonant Raman scattering in ZnO," Physical Review B **16**, 3753 (1977).

[21]M. Rajalakshmi, A. K. Arora, B. Bendre, and S. Mahamuni, "Optical phonon confinement in zinc oxide nanoparticles," Journal of Applied Physics **87**, 2445–2448 (2000).

[22]Y. Liu, H. Zhang, X. An, C. Gao, Z. Zhang, J. Zhou, M. Zhou, and E. Xie, "Effect of Al doping on the visible photoluminescence of ZnO nanofibers," Journal of Alloys and Compounds **506**, 772–776 (2010).

[23]K. Samanta, P. Bhattacharya, and R. S. Katiyar, "Raman scattering studies of p-type Sb-doped ZnO thin films," Journal of Applied Physics **108**, 113501 (2010).

[24]S. Limpijumnong, S. Zhang, S.-H. Wei, and C. Park, "Doping by large-size-mismatched impurities: the microscopic origin of arsenic-or antimony-doped p-type zinc oxide," Physical Review Letters **92**, 155504 (2004).

[25]S. Sharma and G. Exarhos, "Raman spectroscopic investigation of ZnO and doped ZnO films, nanoparticles and bulk material at ambient and high pressures," *Solid State Phenomena* (Trans Tech Publ, 1997), pp. 32–37.

[26]C. Lin, S. Young, C. Kung, L. Horng, H. Chen, M. Kao, Y. Shih, and C. Ou, "Phonon spectra and magnetic behaviors of hydrothermally synthesized Sm-doped ZnO nanorods," Vacuum **87**, 178–181 (2013).

[27]F. Otieno, M. Airo, R. M. Erasmus, D. G. Billing, A. Quandt, and D. Wamwangi, "Structural and spectroscopic analysis of ex-situ annealed RF sputtered aluminium doped zinc oxide thin films," Journal of Applied Physics **122**, 075303 (2017).

[28]X. Meng, D. Zhao, D. Shen, J. Zhang, B. Li, X. Wang, and X. Fan, "ZnO nanorod arrays grown under different pressures and their photoluminescence properties," Journal of Luminescence **122**, 766–769 (2007).

[29]Y. Wang, J. Piao, Y. Lu, S. Li, and J. Yi, "Intrinsic ferromagnetism in Sm doped ZnO," Materials Research Bulletin **83**, 408–413 (2016).

[30]J.-C. Ronfard-Haret, D. Kouyate, and J. Kossanyi, "Evidence for direct impact-excitation of luminescent rare-earth centers (Ho^{3+} and Sm^{3+}) in semiconducting zinc oxide," Solid State Communications **79**, 85–88 (1991).

[31]T. Ohtake, S. Hijii, N. Sonoyama, and T. Sakata, "Electrochemical luminescence of n-type ZnO semiconductor electrodes doped with rare earth metals under the anodic polarization," Applied Surface Science **253**, 1753–1757 (2006).

© Author(s) 2019

View publication stats